

# Effective medium modeling to assess gas hydrate and free-gas evident from the velocity structure in the Makran accretionary prism, offshore Pakistan

Ranjana Ghosh · Kalachand Sain

Received: 22 February 2009 / Accepted: 9 March 2009 / Published online: 21 March 2009  
© Springer Science+Business Media B.V. 2009

**Abstract** Seismic properties of sediments are strongly influenced by pore fluids. Stiffness of unconsolidated marine sediment increases with the presence of gas hydrate and decreases with the presence of gas. A strong bottom-simulating reflector (BSR) observed on a seismic profile in the Makran accretionary prism, offshore Pakistan, indicates the presence of gas hydrate and free-gas across the BSR. Elastic properties of gas depend largely on pressure and temperature. We, therefore, first determine the elastic modulus of gas at pressure and temperature calculated at the BSR depth in the study region. The interval velocities derived from the seismic data are interpreted by the effective medium theory, which is a combination of self-consistent approximation and differential effective medium theories, together with a smoothing approximation, for assessment of gas hydrate and free-gas. The results show the saturations of gas hydrate and free-gas as 22 and 2.4% of pore space, respectively, across the BSR.

**Keywords** Gas hydrate · Elastic property · EMT · Interval velocity · Makran offshore

## Introduction

Natural gas hydrates are ice-like crystalline compounds composed of hydrogen-bonded water cages and entrapped “guest” gas (mainly methane) molecules (Sloan 1998, 2003). Gas hydrate is stable at high pressure and moderately low temperature in shallow sediments on the outer

continental margins, deep inland seas and permafrost regions. Huge amounts of methane are believed to be trapped in the form of gas hydrate and as underlying free-gas (Makogon et al. 2007; Klauda and Sandler 2005; Milkov 2004; Ahlbrandt 2002; Kvenvolden 1998a, b). This large reservoir of methane is considered to be a viable source of future energy resource. The dissociation of gas hydrate also has a strong effect on climate change and the sub-sea slope stability (Sloan 1998; Kvenvolden 1998a, b). Therefore, gas hydrate has been a topic of interest to the scientific community from the standpoint of both the resource potential and environmental hazard. Thus, it is essential for the community to develop new methods to identify and quantify gas hydrate by less expensive remote techniques.

Seismic reflection profiling is the best technique for remotely probing hydrate-bearing sediments few hundred meters below sea floor (mbsf) and lying beneath another few hundred meters of water column. The presence of gas hydrate increases both the P- and S-wave seismic velocities of sediments, whereas underlying free-gas reduces the P-wave velocity considerably, but hardly affects the S-wave velocity. Interpreting seismic velocities in order to deduce the amount of gas hydrate requires a relationship between the hydrate fraction in the sediments and the elastic properties of the sediment composites. Till to day, the role of gas hydrate in altering the elastic properties of the hydrate-bearing sediment is not well understood. A range of rock physics models, including (such as): (1) time average equations (Miller et al. 1991; Bangs et al. 1993; Wood et al. 1994); (2) the weighted equation (Lee et al. 1996; Lee and Collett 1999, 2001); (3) the pore-filling model (Hyndman and Spence 1992); (4) the cementation theory (Dvorkin and Nur 1993; Guerin et al. 1999; Sakai 1999); (5) effective medium theories (Helgerud et al. 1999;

R. Ghosh · K. Sain (✉)  
National Geophysical Research Institute (Council of Scientific and Industrial Research), Uppal Road, Hyderabad 500606, India  
e-mail: kalachandsain@yahoo.com

Jakobsen et al. (2000) have been developed to interpret seismic velocity in terms of saturations of gas hydrate and free-gas. The advantage of models based on empirical relations (1–4) is that they are formulated from real data and simple to apply. However, they may not be applicable in areas with rock properties different from where they were formulated.

Here, we model the elastic properties of the sediment and thereby estimate gas-hydrate and free-gas saturations using an effective medium theory (EMT), which is a combination of self-consistent approximation (SCA, Willis 1977) and differential effective medium (DEM, Nishizawa 1982) theory coupled with smoothing approximation. The combined SCA-DEM theory was originally introduced to determine the elastic properties of sedimentary rock (Sheng 1990, 1991) and shale (Hornby et al. 1994). Both SCA and DEM methods find out the effective elastic moduli of a medium from the individual components and their geometry. The effective medium is developed by embedding inclusions of one material within another material. In unconsolidated marine sediments, grains and pore fluids are fully connected (bi-connected medium) at all realistic porosities. However, SCA and DEM separately cannot model bi-connected media at all porosities. SCA produces bi-connectivity within 40–60% porosity but is not valid above 60% porosity. DEM models micro-structure of a medium, but it depends absolutely on whether the starting medium is bi-connected or not. Therefore a bi-connected medium produced by SCA within 40–60% porosity is used as the starting phase and then DEM is used to calculate the effective elastic properties preserving the bi-connectivity of the medium at all porosities. Jakobsen et al. (2000) modified the theory to determine the elastic property of gas hydrate-bearing sediment, an approach which we follow for our modeling. Later, Taylor and Singh (2002) applied the EMT to find out the microscopic properties of magma bodies. Chand et al. (2004) has shown a general comparison between the EMT and other rock physics models through field examples.

Seismic reflection data acquired in the Makran accretionary prism, Arabian Sea (Fig. 1a) indicates gas hydrate and free-gas (Minshull and White 1989; Sain et al. 2000) across a strong bottom simulating reflector (BSR; Fig. 1b) at the depth  $\sim 510$  mbsf. The EMT is applied to determine the elastic properties of the sediment in order to quantify the gas hydrate and free-gas using the derived interval velocity across the BSR.

### Geology of the Makran accretionary prism

The Makran accretionary prism (Fig. 1a) originated as a result of the subduction of the Arabian plate under the Eurasian plate throughout the Cenozoic (Harms et al. 1984;

White 1982). The accretionary prism not only grew seaward by accretion of trench fill sediments, but also by progradation of the slope, shelf and coastal plain. The rate of growth of the Makran prism seaward is 10 cm/year (White 1982; Platt et al. 1985). Vernant et al. (2004) used GPS data to estimate convergence velocities of 2.7 cm/year in the western Makran. The sedimentary rocks within the accretionary complex are largely recycled from the material eroded from the India–Eurasia collision belt and the Late Oligocene to Middle Miocene was characterized by deposition of turbidites along the margins of southeastern Iran and southwestern Pakistan (Fruehn et al. 1997). The modern Makran accretionary prism has developed since the Late Miocene (Platt et al. 1985, 1988). The sediments entering the deformation front of the Makran accretionary prism consist of a lower section of about 4 km thick interpreted to be the Himalayan Turbidites derived from the Indus fan to the east (Kopp et al. 2000) together with an upper 3 km thick section of the Makran Sands derived from the north. The Makran Sands lie unconformably above the Himalayan Turbidites and are themselves covered by a thin layer of shelf deposits. The Makran Sands unit (Middle Miocene to Pliocene Makran) is assumed to consist largely of detritus eroded from the growing Makran wedge itself, from the Oman Mountains to the southwest (Schluter et al. 2002) and also from the hinterland (Grando and McClay 2007).

Mud volcanoes have been found in several places along the Makran coast. These are formed by gas-charged water escaping to the surface (Minshull and White 1989; Schluter et al. 2002). Accreted sediments show significantly higher vertical velocity gradients than those of sediments entering the prism; this change is interpreted as due to porosity reduction as pore fluids are squeezed out of the compacting sediments. The seismic evidence suggests a two-stage compaction process, with rapid initial dewatering through intergranular permeability as sediment enters the prism followed by a build up of pore pressure as the permeability decreases and fluid migration is restricted to fault zones (Minshull and White 1989).

### EMT modeling

It is assumed clay platelets form the skeleton of the sediment and is oriented in different directions but aligned locally. Since the elastic properties of minerals like calcite, feldspar, silt etc. are almost similar to that of quartz (Jakobsen et al. 2000), we have approximated quartz as the isolated inclusion or unconnected solid part of the matrix, which even at relatively high concentration does not form the connected phase. The modeling procedure of Jakobsen et al. (2000) is adapted for gas hydrate bearing sediment and discussed here. According to this theory two end

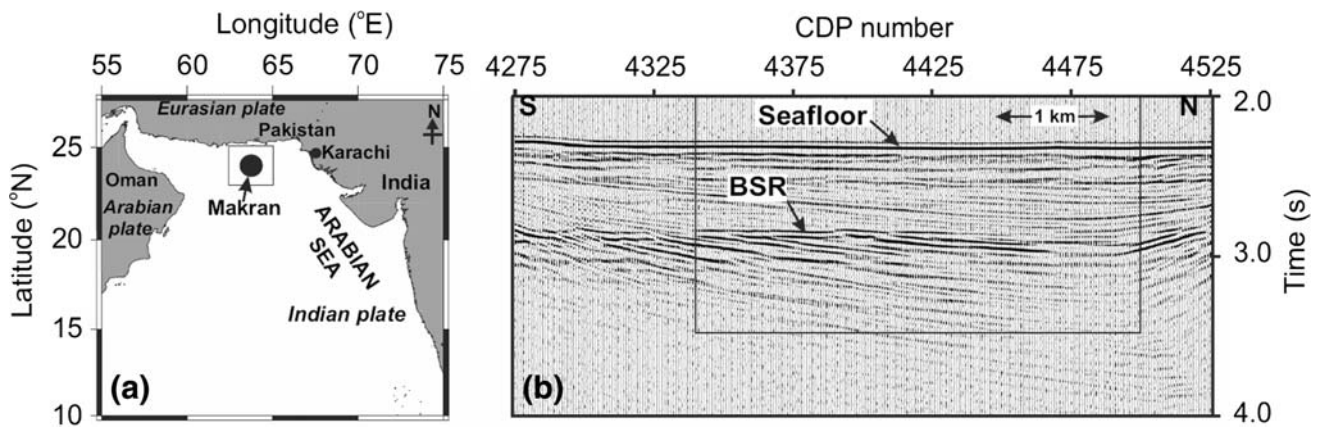


**Fig. 1** **a** The location of study area in the Makran accretionary prism and **b** Seismic stacked section between CDPs 4,275–4,525, showing the BSR and seafloor. CDPs 4,340–4,500, used for estimation of gas hydrate and free-gas are shown by a box

member distributions of gas hydrate are considered: (1) non-contact model- if gas hydrate occupies the pore space without appreciable grain contact. In this model, gas hydrate is a part of the pore fluid (Fig. 2a) and (2) contact model- if gas hydrate forms a continuous matrix and cements and coats the grain. In this model, gas hydrate is a part of matrix (Fig. 2b). Roles of water and gas hydrate are exchanged in these gas hydrate models.

The clay platelets in marine sediments commonly have a preferred horizontal alignment which shows anisotropic elastic behavior in the long wavelength (Hornby et al. 1994; Jakobsen et al. 2000). The clay platelets may orient from completely aligned (transversely isotropic) to completely random (isotropic). The degree of anisotropy depends on the specific orientation distribution of the clay-

platelets (Jakobsen et al. 2000; Hornby et al. 1994; Sayers 1994).

Non-contact model of gas hydrate

The starting medium for this model is composed of water and clay whose effective elastic moduli are calculated by the SCA/DEM method. Gas hydrate is then included by replacing water (leaving the clay concentration unchanged) until the desired gas hydrate concentration is achieved. Here, the effective microstructure is connected clay (load-bearing), connected water and unconnected gas hydrate (non-load-bearing). Gas hydrate has the same aspect ratio (1/20) and orientation as the clay platelets (Hornby et al. 1994; Jakobsen et al. 2000).

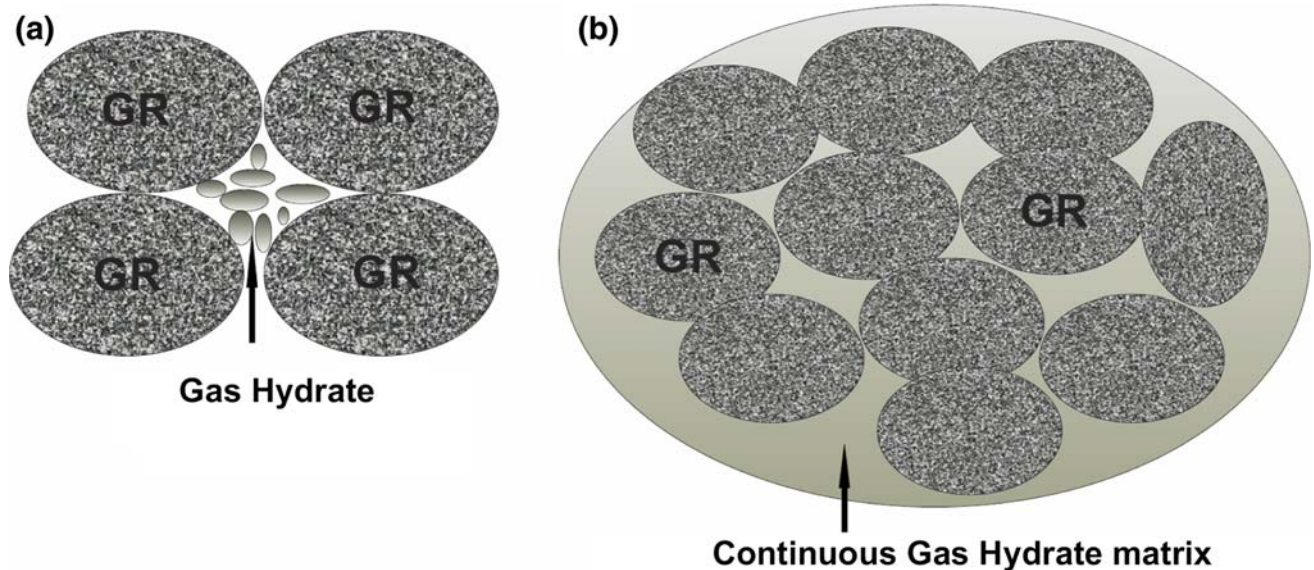


**Fig. 2** Distribution of gas hydrate in pore space: **a** gas hydrate replaces pore-fluid—Non-contact model and **b** gas hydrate cements and coats grain—Contact-cementing model

## Contact model of gas hydrate

The role of gas hydrate and water are reversed for the contact model with respect to the non-contact model. The starting composite is clay–gas hydrate instead of clay–water as in the case of non-contact model. The elastic moduli are computed using combined SCA-DEM theory with water replacing gas hydrate. The effective micro-structure of this procedure is connected (load-bearing) clay, connected (load-bearing) gas hydrate, and unconnected (extremely low permeability, undrained stiffnesses) water.

After incorporating the anisotropy due to orientation distribution pattern of clay platelets, quartz is included in the aggregated clay–water–gas hydrate composite using the DEM method. The concentration of quartz is increased successively from zero to the desired volume replacing all other constituents in proportion to the volume fraction of the inclusion (quartz) and other constituents. A spherical inclusion model (aspect ratio of one) is used for quartz (Jakobsen et al. 2000; Hornby et al. 1994).

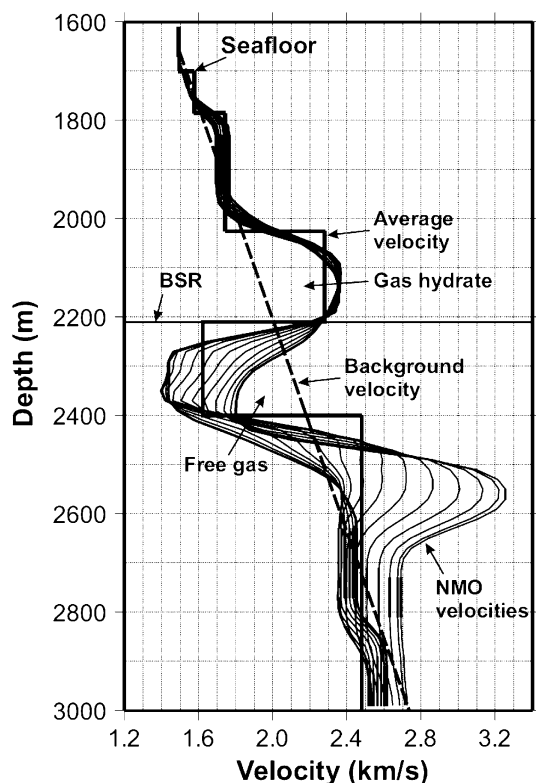


**Fig. 3** Thin lines show smooth NMO interval velocity–depth functions at 10 CDP intervals between CDPs 4,340 and 4,500. Thick solid line shows averaged interval velocity with depth. Dashed line is a straight line fitted to the averaged interval velocity, considered as the background velocity

## Free-gas estimation

Free-gas is included in the clay–water composite using the DEM theory by replacing water leaving clay unchanged. Then quartz is included in the clay–water–gas composite.

The velocity of the effective medium for each case is computed from the effective stiffness coefficients (Jakobsen et al. 2000) of the sediment.

## Methods and results

### Derivation of velocity–depth function

We derive the normal move out (NMO) interval velocities (Fig. 3) across the BSR at 10 common depth point (CDP) intervals between CDPs 4,340 and 4,500 (Fig. 1b). Increase in seismic velocities above the BSR and decrease in velocities below the BSR clearly indicate the presence of gas hydrate and free-gas. Because the NMO-derived velocities are not very accurate, the average of these velocities within the shallow depth across the BSR can be considered to be representative of the velocity structure for the study region. A straight line (Fig. 3) is fitted to the averaged interval velocity–depth function in order to obtain a background (no hydrate/no free-gas) velocity–depth trend. We use the background velocity of  $\sim 2$  km/s at the BSR depth of 510 mbsf (Fig. 3) for estimating gas hydrate and free gas from the averaged interval velocity–depth function.

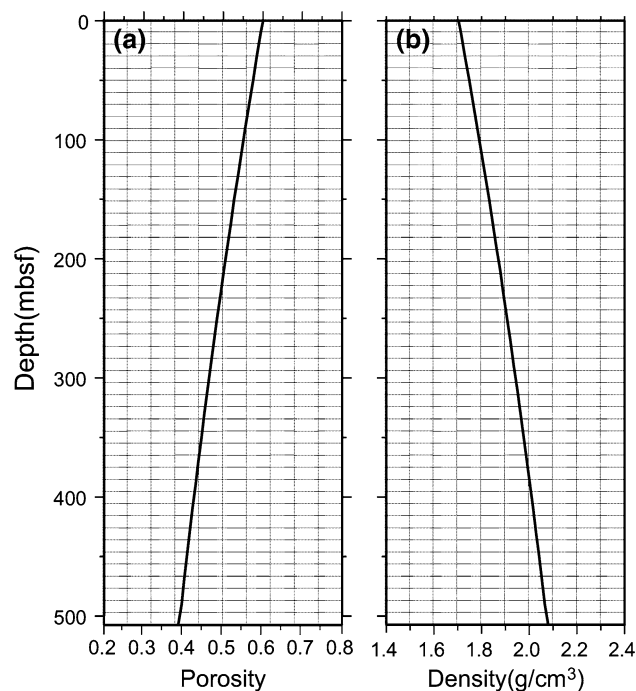


**Fig. 4** a Porosity–depth function and b Density–depth function

**Table 1** Densities ( $\rho$ ), P-wave ( $V_p$ ) and S-wave ( $V_s$ ) velocities of different constituents used (Jakobsen et al. 2000) for modeling

Constituents	$\rho$ (g/cm <sup>3</sup> )	$V_p$ (m/s)	$V_s$ (m/s)
Clay	2.60	3,400	1,600
Water	1.00	1,500	0000
Hydrate	0.92	3,800	2,000
Quartz	2.70	5,980	4,040

Porosity–depth function

Porosity–depth function (Fig. 4a) is computed from the well-known Athy’s law (Athy 1930) as:

$$\phi = \phi_0 e^{-(Z/\lambda)} \tag{1}$$

where,  $\phi_0 = 0.6$  is the seafloor porosity and  $\lambda = 1.17/\text{km}$  is the compaction factor (Minshull and White 1989).

Fractions of minerals of the matrix

The background velocity depth function (Fig. 3) can be represented as:

$$V_p = 1,530 + 0.931 \times D \tag{2}$$

where, the seafloor (at 1,700 m water depth) velocity is 1,530 m/s and velocity gradient is 0.931/s.

The major mineralogical constituents of the sediment are assumed to be clay, which constitutes the building blocks, and quartz (silt minerals), which is the isolated inclusion even at higher concentration. The elastic parameters of different constituents of the sediment, used in our calculation, are shown in Table 1. At 510 mbsf, the velocity of water-filled sediment is computed using the EMT (Hornby et al. 1994; Jakobsen et al. 2000) with different fractions of clay and quartz, which are then matched with the background velocity. We find that the random distribution of clay platelets with respect to the normal to the horizontal plane gives a better fit with the background velocity for this region, which exhibits isotropic behavior of the sediment. The random orientation distribution function (ODF) of clay plates is characterized by the coefficients  $W_{200} = 0$  and  $W_{400} = 0$  in the Legendre polynomial (Sayers 1994). 13.5% clay and 86.5% quartz with porosity of 39% match with the background velocity of 2 km/s at the BSR depth (510 mbsf). These mineralogical constituents predict that the sediment in the Makran accretionary prism is mostly sandy in nature.

Density–depth function

The background density variation with depth is calculated using the relationship between porosity and bulk density ( $\rho_b$ ) as:

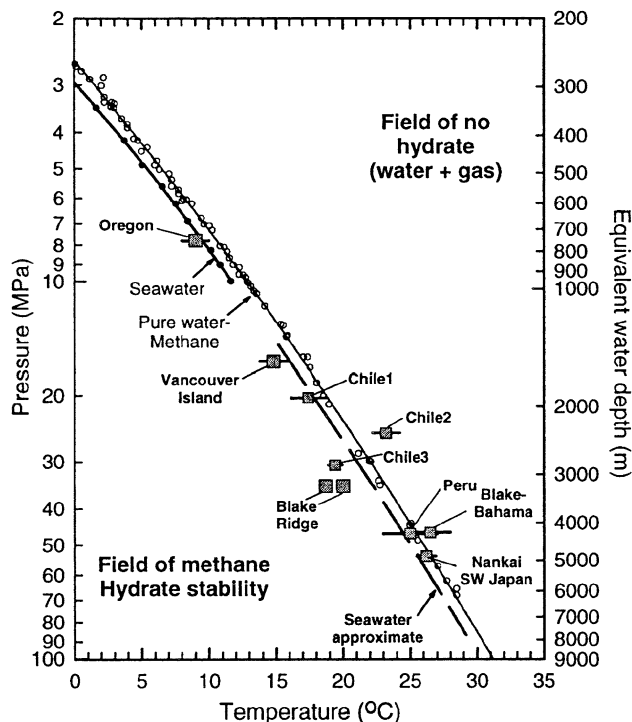


**Fig. 5** Pressure temperature phase diagram of gas hydrate (after Ganguly et al. 2000)

$$\rho_b = \rho_w \phi + \rho_c v_c (1 - \phi) + \rho_q v_q (1 - \phi) \tag{3}$$

where, densities and volume concentrations of water, clay, quartz are respectively  $\rho_w = 1 \text{ g/cm}^3$ ,  $\rho_c = 2.6 \text{ g/cm}^3$ ,  $\rho_q = 2.7 \text{ g/cm}^3$  and  $v_w =$  volume of water (=porosity),  $v_c =$  volume of clay,  $v_q =$  volume of quartz. Figure 4b shows the density–depth function of the study area. The average density in this region is calculated as  $1.94 \text{ g/cm}^3$ .

Pressure and temperature

The average depth of the seafloor observed in the seismic section is 1,700 m (Sain et al. 2000). Total pressure ( $P_T = \rho g z$ ) exerted down to the depth of BSR (510 mbsf) is the sum of the pressure due to the water column and the sedimentary column from the seafloor to the BSR depth, which is calculated as 26.34 MPa. The temperature corresponding to this pressure at this depth is calculated from the pressure temperature phase diagram (Fig. 5) of gas hydrates as  $\sim 21^\circ\text{C}$ .

Density and bulk modulus of gas

Elastic properties of gas depend greatly on the pressure and temperature of the surrounding medium. We, therefore, determine the elastic modulus of gas for particular pressure and temperature calculated at the BSR depth. The density and bulk modulus of gas are calculated from the

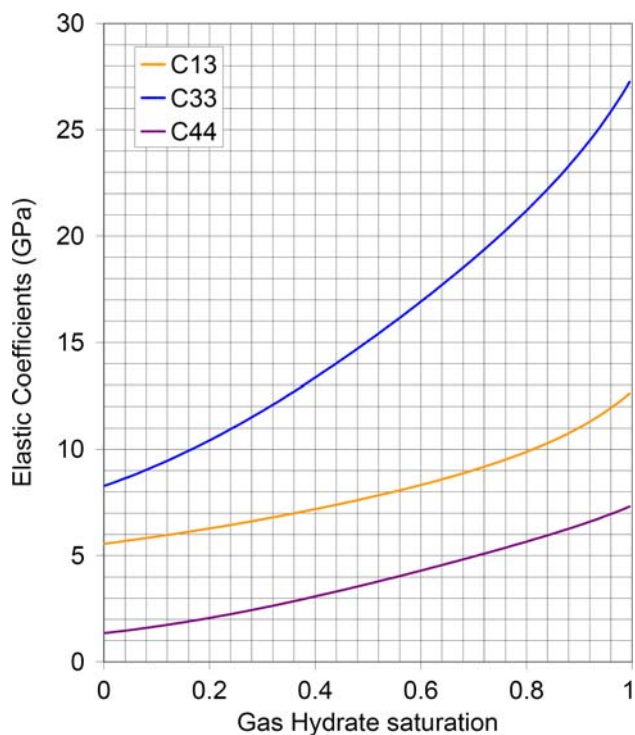


**Fig. 6** Elastic coefficients with gas hydrate saturation, determined from the effective medium theory at 13.5% clay, 86.5% quartz and 39% porosity

relationship given by Batzle and Wang (1992). We estimate density and the bulk modulus of gas as  $0.2 \text{ g/cm}^3$  and  $67 \text{ MPa}$  for the determined pressure  $26.34 \text{ MPa}$  and temperature  $21^\circ\text{C}$  at the BSR depth.

#### Gas hydrate and free-gas concentrations

The elastic properties of gas hydrate can be considered to be stable with pressure and temperature. Therefore, we take the elastic moduli of gas hydrate from the published literature (Table 1). The gas hydrate saturation is estimated using the combined SCA-DEM theory proposed by Jakobsen et al. (2000), taking the orientation of gas hydrate to be similar to that of clay platelets. The elastic properties of gas hydrate-bearing sediment have been determined for both gas hydrate as a part of pore fluid (non-contact model) and gas hydrate as a part of matrix (contact model). But the model, considering gas hydrate as a part of matrix, does not provide any estimation of gas hydrate from the observed velocity (derived NMO velocity). Thus the role of gas hydrate for this region is non-load-bearing (non-contact model). The effective media is isotropic, defined by three coefficients of the stiffness tensor  $C$  as  $C_{11} = C_{22} = C_{33}$ ,  $C_{44} = C_{55} = C_{66}$ ,  $C_{12} = C_{21} = C_{13} = C_{31} = C_{23} = C_{32}$ . Figure 6 shows that the stiffness coefficients of the effective medium, composed of clay, quartz, water and gas

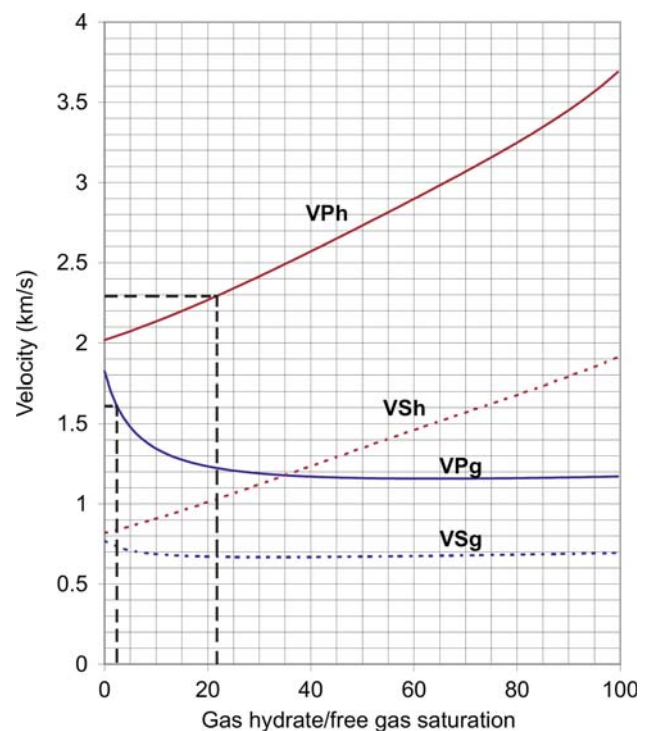


**Fig. 7** Variation of P-wave ( $VP$ ) and S-wave ( $VS$ ) velocities with gas hydrate ( $h$ ) and free-gas ( $g$ ) saturations at 13.5% clay, 86.5% quartz and 39% porosity. Dashed black lines show the saturations of gas hydrate (22%) and free-gas (2.4%) across the BSR

hydrate, increase with gas hydrate saturation. Gas is included as replacing water in a similar way as gas hydrate is included. The determined bulk modulus and density of gas are used for estimating concentration of free-gas. Figure 7 shows the variation of elastic velocities computed by the EMT with gas hydrate and free-gas saturation. The gas hydrate and free-gas saturations are estimated as being 22 and 2.4% of the pore space, respectively, across the BSR, corresponding to a velocity increase of  $2.29 \text{ km/s}$  and a drop of  $1.61 \text{ km/s}$  respectively (Fig. 7).

#### Discussion and conclusions

The determined mineralogy demonstrates that the sediments in the study area are sandy/silty. In the EMT, the assumption of random distribution of clay platelets gives a better fit with the observed background velocity, which exhibits an isotropic behavior for the sediment. Though the EMT is widely used to estimate gas-hydrate saturation in the case of clay-rich marine sediment, here we establish that the theory also works for sand-rich sediment. We have compared the saturations, estimated from the EMT based on combined SCA-DEM theory, with those estimated using the simple EMT proposed by Helgerud et al. (1999). According to the simple EMT, gas hydrate is a component

of the dry frame (load-bearing), increase of which reduces the porosity and alters the solid phase elastic property. From this theory, clay is determined as 10% of solid part, and gas hydrate and free-gas are estimated as 31.3 and 4.14% of pore space, respectively, across the BSR. Considering gas hydrate as a part of matrix, the present model does not give any finite hydrate saturation from the observed velocity. However, using the pore fluid model (non-contact), we estimate the saturation of gas hydrate as 22% of the pore space. Free-gas below the BSR is estimated as 2.4% of pore volume. Thus, we see that the simple EMT satisfies the role of gas hydrate as a part of matrix and the EMT based on SCA/DEM theory supports gas hydrates as a part of pore fluid. Both the models are physics-based, which can be applied to the gas hydrate-bearing marine sediments. But the model of Helgerud et al. (1999) is limited if the critical porosity is assumed to be 0.35, whereas, the model of Jakobsen et al. (2000) determines the elastic property of the sediment at any finite porosity.

Coexistence of water, gas hydrate and free-gas is also possible (Guerin et al. 1999; Kumar et al. 2007; Lee and Collett 2006). This may be explained by capillary effects in smaller pores or the remaining crystalline structure after partial decomposition of gas hydrate (Guerin et al. 1999). The strong BSR observed in the seismic section in the Makran accretionary prism clearly indicates a sharp boundary between gas hydrate-bearing sediment above and free-gas-bearing sediment below the BSR. Therefore, in this paper we do not model the case for coexistence of water, gas hydrate and gas.

Ojha and Sain (2008) estimated gas hydrate and free-gas from the  $V_p/V_s$  ratio, obtained by traveltimes inversion coupled with amplitude modeling, as 12.0–14.5% and 4.5–5.5% respectively, using the rock physics based on the Biot-Gassman theory modified by Lee (Lee 2002). These authors further estimated gas hydrate and free-gas as 13–20% and 3–3.5% respectively using the rock physics model of Helgerud et al. (1999). Major discrepancies in estimations of gas hydrate and free-gas arise from the chosen rock physics theories and values of elastic constants of the constituents of sediment. Figure 3 shows a large amount of free-gas within the 200-m-thick sedimentary column. This gas may have resulted from the dissociation of pre-existing gas hydrate as a result of the upward movement of the stability field, caused by rapid sedimentation and tectonic uplift in this area. Based on the estimates from either of the rock physics theories, we conclude that the Makran accretionary prism may be a large reservoir of methane gas trapped within and below the gas hydrate bearing sediment.

In this paper gas hydrate and free gas are estimated from the seismic P-wave velocity derived from the NMO

analysis of the multichannel surface seismic data. S-wave velocity can be determined by amplitude versus offset (AVO) modeling (Ojha and Sain 2008), which is beyond the scope of this paper.

**Acknowledgments** We are grateful to the Director, NGRI for his kind consent to publish this work. We thank two anonymous reviewers and Dr. Peter D. Clift for their constructive comments/suggestions to improve the manuscript. CSIR, New Delhi is acknowledged for financial support through Senior Research Fellowship to RG.

## References

- Ahlbrandt TS (2002) Future petroleum energy resources of the world. *Int Geol Rev* 44:1092–1104
- Athy LF (1930) Density, porosity and compaction of sedimentary rocks. *AAPG Bull* 14:1–24
- Bangs NLB, Sawyer DS, Golovchenko X (1993) Free-gas at the base of the gas hydrate zone in the vicinity of the Chile triple junction. *Geology* 21:905–908
- Batzle W, Wang Z (1992) Seismic properties of pore fluids. *Geophysics* 57:1396–1408
- Chand S, Minshull TA, Gei D, Carcione JM (2004) Elastic velocity models for gas-hydrate-bearing sediments—a comparison. *Geophys J Int* 159:573–590
- Dvorkin J, Nur A (1993) Rock physics for characterization of gas hydrate. In: Howell DG (ed) *The future of energy gases: United States Geological Survey Professional Paper 1570* pp 293–298
- Fruehn J, White RS, Minshull TA (1997) Internal deformation and compaction of the Makran accretionary wedge. *Terra Nova* 9:101–104
- Ganguly N, Spence GD, Chapman NR, Hyndman RD (2000) Heatflow variations from bottom simulating reflectors on the Cascadia margin. *Mar Geol* 164:53–68
- Grando G, McClay K (2007) Morphotectonics domains and structural styles in the Makran accretionary prism, offshore Iran. *Sed Geol* 196:157–179
- Guerin G, Goldberg D, Meltser A (1999) Characterization of in situ elastic properties of gas hydrate-bearing sediments on the Blake Ridge. *J Geophys Res* 104:17781–17795
- Harms JC, Cappel HN, Francis DC (1984) The Makran coast of Pakistan; its stratigraphy and hydrocarbon potential. In: Haq BU, Milliman JD (eds) *Marine geology and oceanography of Arabian Sea and coastal Pakistan*. Van Nostrand Reinhold, New York, pp 3–26
- Helgerud MB, Dvorkin J, Nur A (1999) Elastic-wave velocity in marine sediments with gas hydrates: effective medium modeling. *Geophys Res Lett* 26:2021–2024
- Hornby BE, Schwartz LM, Hudson JA (1994) Anisotropic effective medium modeling of the elastic properties of shales. *Geophysics* 59:1570–1583
- Hyndman RD, Spence GD (1992) A seismic study of methane hydrate marine bottom simulating reflectors. *J Geophys Res* 97:6683–6698
- Jakobsen M, Hudson JA, Minshull TA, Singh SC (2000) Elastic properties of hydrate-bearing sediments using effective medium theory. *J Geophys Res* 105:561–577
- Klauda JB, Sandler SI (2005) Global distribution of methane hydrate in ocean sediment. *Energy Fuels* 19:459–470
- Kopp C, Fruehn J, Flueh ER, Reichert C, Kukowski N, Bialas J, Klaeschen D (2000) Structure of the Makran subduction zone

- from wide-angle and reflection seismic data. *Tectonophysics* 329:171–191
- Kumar D, Sen MK, Bangs NL (2007) Gas hydrate concentration and characteristics within hydrate ridge inferred from multicomponent seismic reflection data. *J Geophys Res* 112:B12306
- Kvenvolden KA (1998a) A primer on the geological occurrence of gas hydrate. In: Henriert JP, Mienert J (eds) *Gas hydrates: relevance to the world margin stability and climate change*. Geol Soc, London, pp 9–30 Special Publications 37
- Kvenvolden KA (1998b) Methane hydrate- A major reservoir of carbon in the shallow geosphere? *Chem Geol* 71:41–51
- Lee MW (2002) Biot-Gassmann theory for velocities of gas hydrate bearing sediments. *Geophysics* 67:1711–1719
- Lee MW, Collett TS (1999) Amount of gas hydrate estimated from compressional and shear wave velocities at the JAPEX/JNOC/GSC Mallik 2L–38 Gas hydrate Research well. In: Dallimore SR, Uchida T, Collett TS (eds) *Scientific results from JAPEX/JNOC/GSC Mallik 2L-38 gas hydrate research well, Mackenzie Delta*, vol 544. *Geol Sur Can Bull*, Northwest Territories, Canada, pp 313–322
- Lee MW, Collett TS (2001) Comparison of elastic velocity models for gas hydrate-bearing sediments. In: Paull CK, Dillon WP (eds) *Natural gas hydrates: occurrence, distribution and detection*, American geophysical union geophysical monograph vol 124. American Geophysical Union, Washington, pp 179–188
- Lee MW, Collett TS (2006) Gas hydrate and free-gas saturations estimated from velocity logs on hydrate ridge, offshore Oregon, USA. In: Tréhu AM, Bohrmann G, Torres ME, Colwell FS (eds) *Ocean Drilling Program, Proc ODP, Sci Results*, vol 204, College Station pp 1–25
- Lee MW, Hutchinson DR, Collett TS, Dillon WP (1996) Seismic velocities for hydrate-bearing sediments using weighted equation. *J Geophys Res* 101:20347–20358
- Makogon YF, Holditch SA, Makogon TY (2007) Natural gas hydrates—a potential energy source for the 21st Century. *J Petrol Sci Eng* 56:14–31
- Milkov AV (2004) Global estimates of hydrate-bound gas in marine sediments: how much is really out there? *Earth Sci Rev* 66:183–197
- Miller JJ, Lee MW, von Huene R (1991) An analysis of a seismic reflection from the base of a gas hydrate zone, offshore Peru. *AAPG Bull* 75:910–924
- Minshull TA, White RS (1989) Sediment compaction and fluid migration in the Makran accretionary prism. *J Geophys Res* 94:7387–7402
- Nishizawa O (1982) Seismic velocity anisotropy in a medium containing oriented cracks: transversely isotropic case. *J Phys Earth* 30:331–347
- Ojha M, Sain K (2008) Appraisal of gas hydrate/free-gas from  $V_p/V_s$  ratio in the Makran accretionary prism. *Mar Pet Geol* 25:637–644
- Platt JP, Leggett JK, Young J, Raza H, Alam S (1985) Largescale sediment underplating in the Makran accretionary prism, Southwest Pakistan. *Geology* 13:507–511
- Platt JP, Leggett JK, Alam S (1988) Slip vectors and fault mechanics in the Makran accretionary wedge, Southwest Pakistan. *J Geophys Res* 93:7955–7973
- Sain K, Minshull TA, Singh SC, Hobbs RW (2000) Evidence for a thick free-gas layer beneath the bottom simulating reflector in the Makran accretionary prism. *Mar Geol* 164:37–51
- Sakai A (1999) Velocity analysis of vertical seismic profile (VSP) survey at JAPEX/JNOC/GSC Mallik 2L-38 Gas hydrate research well, Mackenzie Delta, Northwest Territories, Canada. In: Dallimore SR, Uchida T, Collett TS (eds) *Geol Sur Can Bull volume 544*, pp 323–340, *Geol Sur Can*, Ottawa
- Sayers CM (1994) The elastic anisotropy of shales. *J Geophys Res B1* 99:767–774
- Schluter HU, Prexl A, Gaedicke C, Roeser H, Reichert C, Meyer H, von Daniels C (2002) The Makran accretionary wedge; sediment thicknesses and ages and the origin of mud volcanoes. *Mar Geol* 185:219–232
- Sheng P (1990) Effective medium theory of sedimentary rocks. *Phys Rev B* 41:4507–4512
- Sheng P (1991) Consistent modeling of the electrical and elastic properties of sedimentary rocks. *Geophysics* 56:1236–1243
- Sloan ED (ed) (1998) *Clathrate hydrate of natural gases*. Marcel Dekker, New York
- Sloan ED (2003) Fundamental principles and applications of natural gas hydrates. *Nature* 426:353–359
- Taylor MAJ, Singh SC (2002) Composition and microstructure of magma bodies from effective medium theory. *Geophys J Int* 149:15–21
- Vernant P, Nilforoushan FHD, Abbassi MRVC, Masson FNH, Martinod JAA, Bayer RTF, Chery J (2004) Present-day crustal deformation and plate kinematics in the Middle East constrained by GPS measurements in Iran and northern Oman. *Geophys J Int* 157:381–398
- White RS (1982) Deformation of the Makran accretionary sediment prism in the Gulf of Oman (North-West Indian Ocean). In: Leggett JK (ed) *Trench-Forearc geology: sedimentation and tectonics on modern and ancient active plate margins*, Conference. *Geol Soc Special Publication* 10, pp 357–372
- Willis JR (1977) Bounds of self-consistent estimates for the overall properties of anisotropic composites. *J Mech Phys Solids* 25:185–202
- Wood WT, Stoffa PL, Shipley TH (1994) Quantitative detection of methane hydrate through high-resolution seismic velocity analysis. *J Geophys Res* 99:9681–9695